Ignition Thresholds and Initiation of Pyrolysis from High Flux Exposures

Alexander L. Brown[a*], Jeffrey D. Engerer[b]. Allen J. Ricks[c],

[a]Sandia National Laboratories, PO Box 5800, Albuquerque, 87185, USA, albrown@sandia.gov

[b]Sandia National Laboratories, PO Box 5800, Albuquerque, 87185, USA, jdenger@sandia.gov

[c]Sandia National Laboratories, PO Box 5800, Albuquerque, 87185, USA, ajricks@sandia.gov

*Corresponding author

Highlights:

- Historical cellulose-based ignition thresholds are evaluated for additional materials
- Prior to ignition, solids are observed to release pyrolytic gases
- With a Martin-based model, the initiation of pyrolysis can represent ignition uncertainty
- A theoretical construct trends well with data, suggesting a good potential model for ignition and the start of pyrolysis

Abstract:

Ignitions of solid materials from very high heat fluxes (>200 kW/m^2) are differentiated from more common lower flux ignition because the required total energy input can be lower, and the process is much faster. Prior work has characterized ignition thresholds via thermal properties of the solids, flux, and fluence. The historical data, however, neglect to provide similar focus on the initiation of pyrolysis. The initiation of pyrolysis is of key relevancy because it represents an absolute threshold below which ignition is of zero probability. It is also a metric of potentially higher reliability for assessing material response because surface material properties such as absorptivity, conductivity, and density tend to change upon initial pyrolysis due to charring or other transformations. Recent data from concentrated solar flux for a variety of materials and exposures are analyzed here to explore the nature of trends and thresholds for onset of pyrolysis at high heat flux. This work evaluates initiation threshold data and provides a theoretical technique for further model development. The technique appears to be functionally appropriate to evaluate trends to aid in predicting material response to high flux exposures.

Keywords: High flux fires, solid combustion, pyrolysis initiation, ignition

1. Introduction

High radiative flux (>200 kW/m^2) can occur in metal fires, propellant accidents, above-ground nuclear detonations, lightning strikes, etc. Historical information that appears very detailed and comprehensive was centered around cellulose ignition thresholds [1-4]. A more critical evaluation of this source data suggests a very detailed examination of darkened cellulose at small (approximately a few centimeters in diameter) exposures, with a more cursory and often questionably sourced evaluation of some other materials. Much of the historical testing of this nature in the open literature was done in the 1950-1960s, with very little additional work since then. There have been many changes to manufacturing and materials since that time with many modern materials that lack detailed characterization in this environment. Consider also the change in experimental test capabilities since the original datasets, which allows for improved interrogation of the tests.

A helpful construct was developed historically that aided in interpreting the cellulose results [1]. The peak ignition flux (or irradiance) and the ignition fluence (fluence being the integration of flux with time, having units of energy per unit area) were strategically scaled by the relevant thermal parameters of the solids being exposed. The normalization was guided by a strategic non-dimensionalization of the data with the key dimensionless parameter relating the thermal and physical properties being the Fourier number ($Fo=\alpha_t t/L^2$, where α_t is the thermal diffusivity [$k/\rho C_P$], t is a characteristic time, L is a characteristic length, k the thermal conductivity, ρ the density, and C_P the specific heat). By semi-nondimensionalization of the flux and fluence, the ignition data from disparate tests of varying thickness and density collapsed to form relatively sharp regime thresholds that delineate between several different observed ignition behaviors and non-ignition. The normalized fluence Q_{norm} is given by

$$Q_{norm} = \alpha_o Q/\rho C_P L \qquad (1)$$

Here α_o is the optical absorptivity, Q is the fluence (the flux integrated over time), and L is the thickness of the sample. The optical absorptivity (α_o) is often assumed constant, but in most applications can be subtly or significantly functional with the surface char fraction and temperature. The normalized irradiance $\dot{Q}_{norm}$ is given by

$$\dot{Q}_{norm} = \alpha_o \dot{Q} L/k \qquad (2)$$

where $\dot{Q}$ is flux or irradiance, usually taken as the maximum to the object. The normalized fluence and flux both have units of temperature.

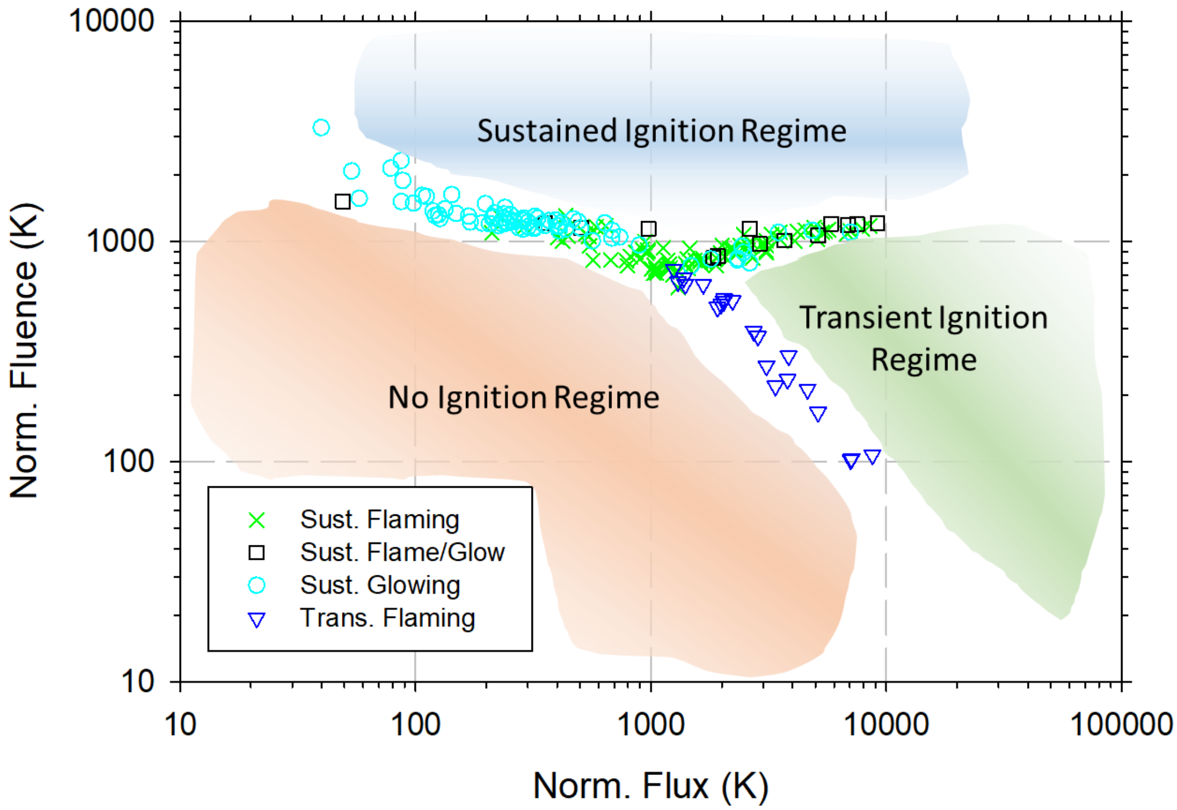

Fig. 1. Cellulose ignition threshold data from Butler (with Martin) et al. [4] with annotated ignition regimes

Fig. 1 shows a reproduction of cellulose ignition threshold data from Butler (with Martin) et al. square-wave exposure profile tests [4]. Starting from the left, there is a branch of data nearly linear with 1000 K normalized fluence, that marks the threshold between no ignition and sustained glowing. At 1000 K normalized irradiance

the trend branches. The upper branch is a sustained flaming branch, while the lower branch is a threshold for transient flaming. Transient flaming means that flaming occurred, but only while the external radiation flux source was being applied. Sustained flaming persisted past the application of the imposed flux. Below a normalized flux of about 100, thermal conductivity and convective losses become increasingly important, and the ignitions occur with increasing normalized fluence below this threshold and become more sensitive to the material geometry. A comparable plot exists for flux profiles inspired by detonations of a nuclear weapon (NW) with thresholds of similar label and shapes from the same research group [2]. These datasets contributed to the most comprehensive and theoretically promising ignition model for high flux scenarios, when compared to other sources of tabulated ignition thresholds [3] or more empirical relations developed based on the existing threshold data. Since the introduction of Martin's map, other ignition modeling methods have become more widely utilized; however, we believe this model is still appropriate and best suited for the high flux regime, where convective and conductive losses and other effects are minimized compared to the radiative flux.

The work of Martin (2004) [2] provides a model for dynamic heat flux for a nuclear weapon, but this flux profile can be difficult to replicate synthetically. Experimentally, a square or trapezoidal flux profile is easier to achieve with concentrated solar power. To illustrate how the exposures relate to the idealized ignition threshold, examples of these two types of wave forms are plotted as flux and fluence versus time in Fig. 2 (top) and projected into normalized flux/fluence space for a posterboard exposure (bottom). The green dashed line is an approximation of Martin's model (Fig. 1). The NW exposure was taken from recommendations of prior studies [2,3]. The flux/fluence plot illustrates three selected isocontours of the Fourier number as dotted lines, which is conveniently the product of the normalized fluence to the normalized flux based on the normalization technique. The target experiences conditions from the lower-left in the plot, and as flux and fluence increase the environment transitions towards the upper-right. When the trend line passes the green dashed line, ignitions are deemed likely based on Martin's experimental work. Flux is considered maximum flux from the exposure and is not decreased with time to plot the trends. Square or trapezoidal wave forms can reasonably replicate the more complex conditions enabling imperfect experiments to still be reasonably approximate of more complex scenarios. Besides the main point of interest, the energy input and flux, there is the question of spectral content of the incident radiation. This will matter for non-gray materials. Solar flux is mostly gray with some absorption lines due to atmospheric gases, and is generally considered a reasonable approximation of most high-flux application emissions [3].

Recently developed datasets provide new opportunities to investigate high heat flux ignition and material response, and a new set of data from concentrated solar energy are now available that augment the knowledge basis for understanding and predicting material behavior under very high radiative heat flux exposures [5-10]. These new data can help improve upon the historical modeling and analytical techniques for estimating material behavior under very high flux conditions.

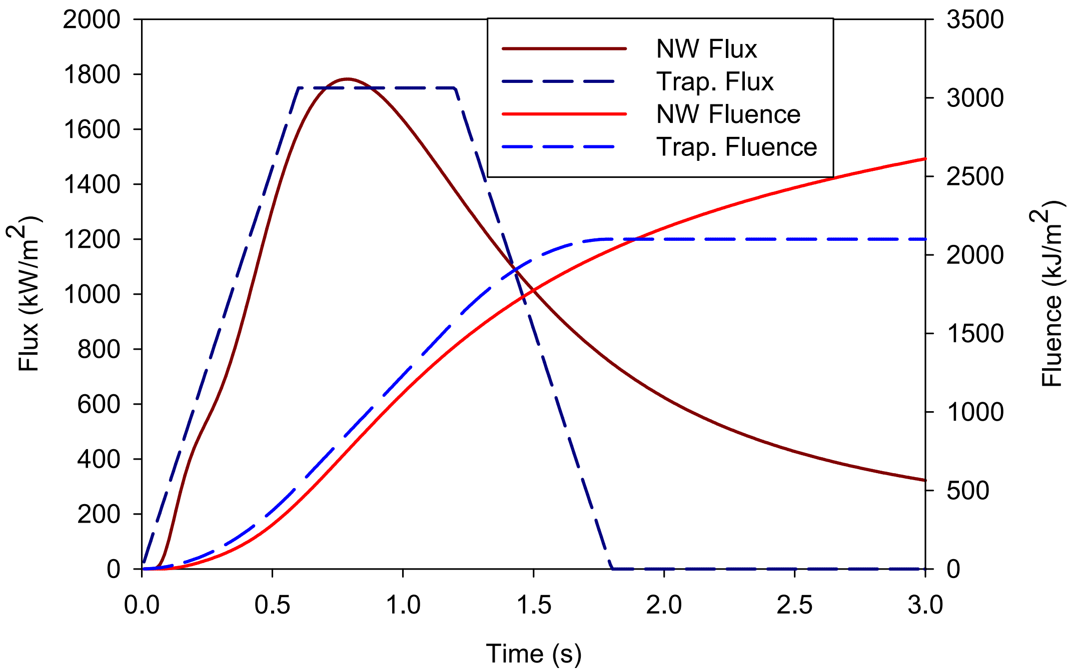

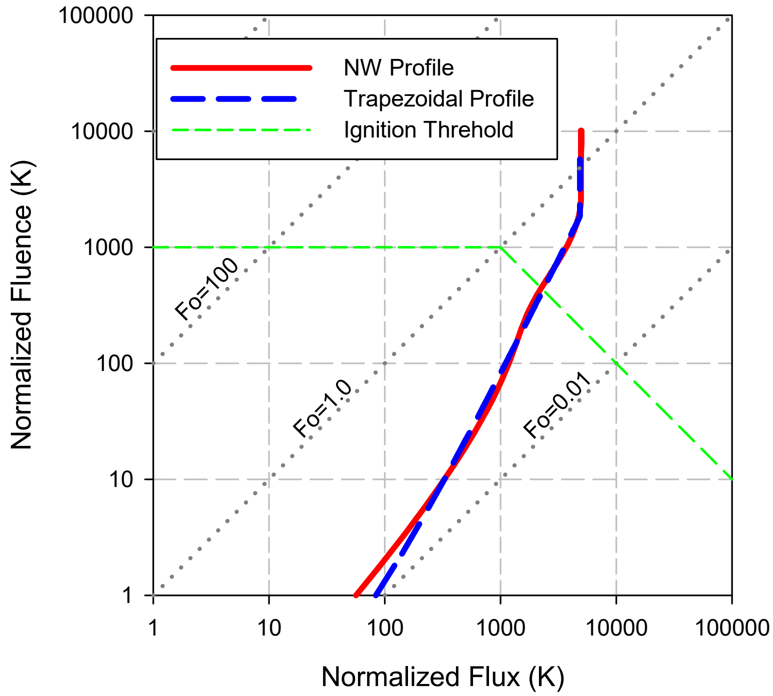

Fig. 2 NW and trapezoidal flux/fluence models plotted (top) and projected onto the normalized flux and fluence map (bottom) for posterboard

This paper describes an analysis effort aimed at interpreting the recent results from several test campaigns. Our test campaign is differentiated from historical work in several key ways:

1. A greater variety of materials are tested at comparable and extended conditions
2. Video data and test characterization permits contributing threshold data from every test that achieves ignition, a much more efficient data collection process than the historical methods
3. Data are also collected on the initiation of pyrolysis, a feature not reported in prior work.

The governing hypothesis for this analysis is that the pyrolysis initiation threshold that was not reported in prior work trends similarly to the historically determined ignition thresholds. The initiation of pyrolysis may be a cleaner threshold than ignition for material characterization in high flux exposure conditions because it is less subject to wind, charring, and radiation shielding issues than ignition. The initiation of pyrolysis should fall below the ignition threshold because it is a pre-ignition requirement. Since prior work omitted mention or description of this feature, this observation represents to our knowledge the first exploration of such a threshold for high flux conditions. Definition of this regime provides new information relevant to predictive capabilities, and the location and shape helps define a new regime.

2. Methods

The National Solar Thermal Test Facility at Sandia National Labs in Albuquerque has two main facilities that concentrate solar energy to generate high flux conditions illustrated in Fig. 3. One is the Solar Tower, which uses a heliostat field (an array of large mirrors with fine motor control that actively track the sun to maintain a relatively constant target location for the rays) to achieve a concentration factor greater than 2000 suns (1 sun is approximately 1 kW/m^2), and a power of 6 MW at length scales of 0.3-1 m. The other is the smaller Solar Furnace which uses a single heliostat and a parabolic dish for smaller length-scale testing (5-7 cm diameter). Several hundred high flux ignition tests have been conducted at these facilities including varying material types, thicknesses and shapes, while also varying flux, fluence, and length-scale. Additional variable parameters include ambient conditions such as wind, humidity, and temperature. Fig. 4 and Fig. 5 show layout sketches suggesting the general arrangement for the tests. Fig. 6 illustrates the pre- and post-test configuration of the shutter system used to create a rapid exposure on test objects. The shutter was used to begin the exposure because the precision mirror adjustments were comparatively slow. At the end of the exposure, the motorized mirrors on the heliostat field were used to end the exposure, being faster for low-precision movement.

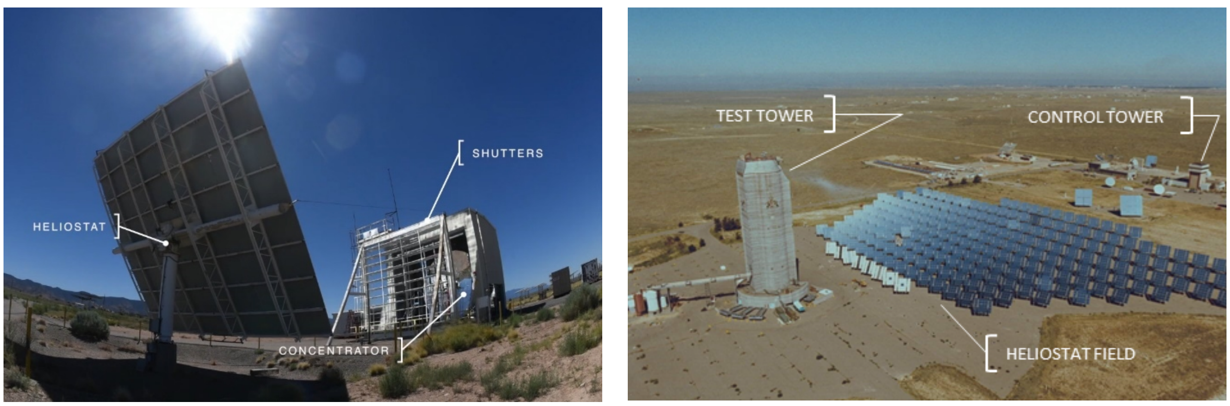

Fig. 3. Annotated photographs of the SF (left) and ST (right) facilities

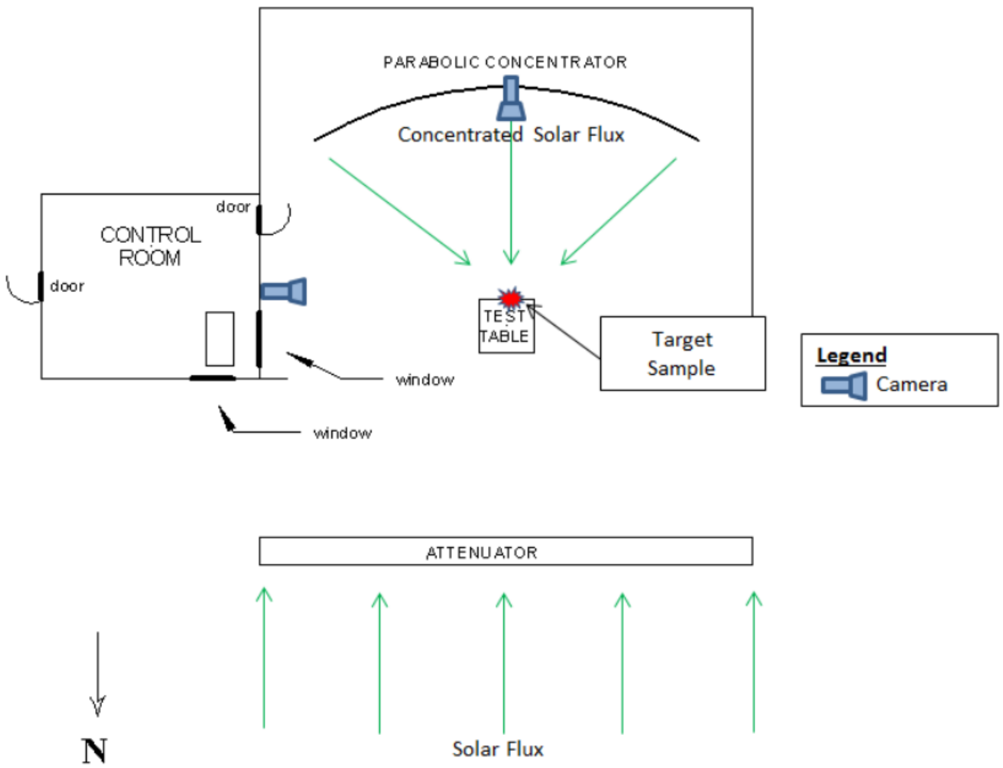

Fig. 4. A general arrangement illustration for the SF tests

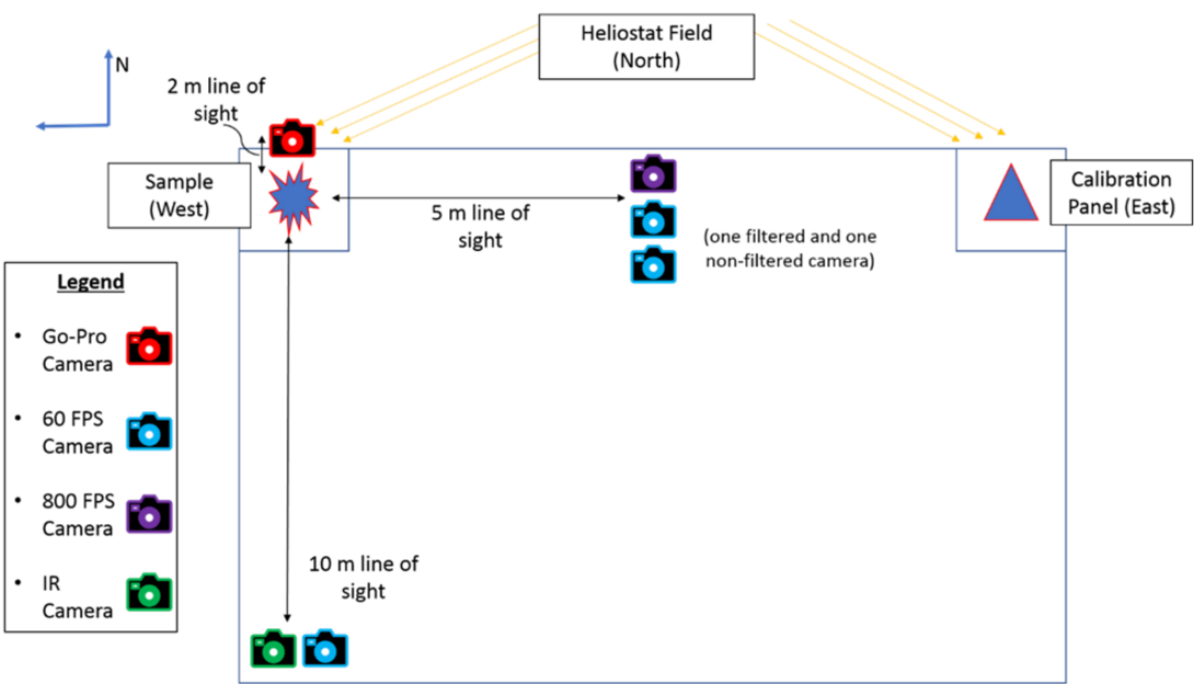

Fig. 5. A general arrangement illustration for the ST tests

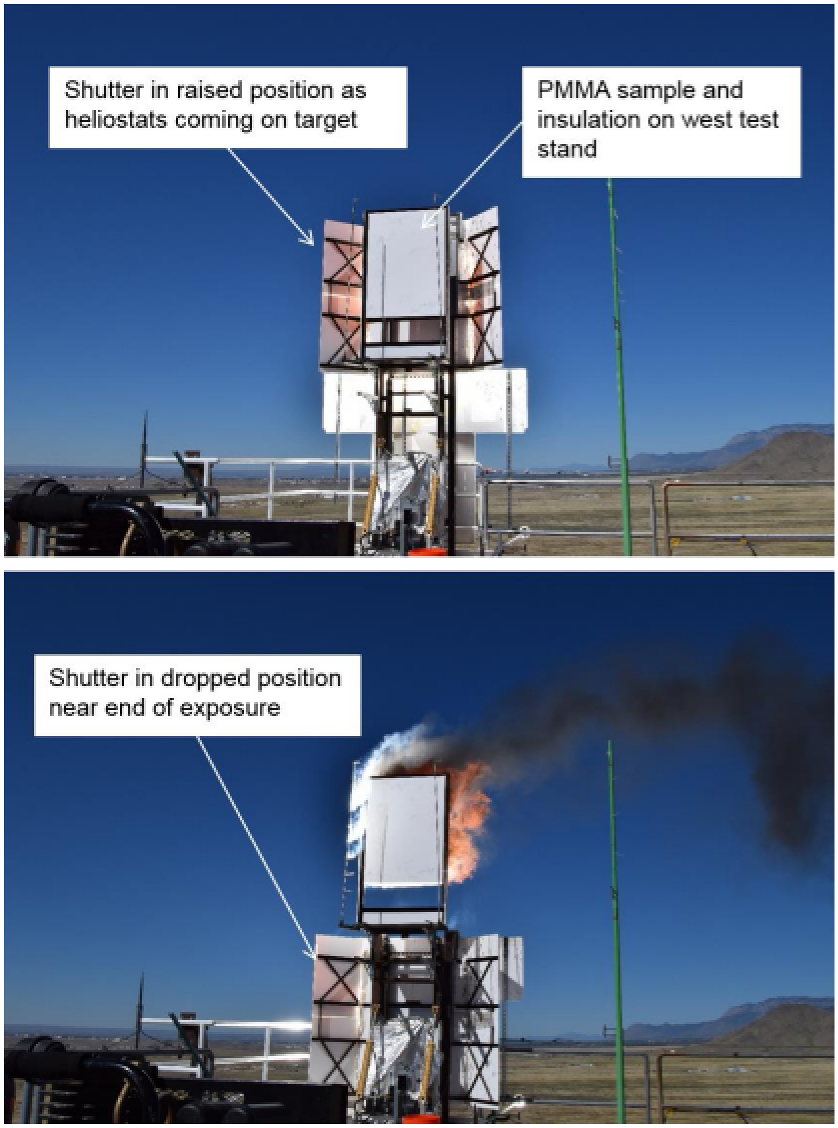

Fig. 6. Photographs illustrating the shutter before (top) and after an exposure on the ST

The data for this study were a component of a test program that involved four phases of testing, three at the Sandia Solar Furnace and one at the Solar Tower. The broader program was not specifically focused on obtaining these data; however, they were available and extracted to support this type of analysis that could not be found in the documentation of the previously taken datasets. The focus of the data from the test phases was broadly defined to support three main objectives. Some data were intended for model validation, in which case samples were tested with a high degree of replicates to capture the aleatoric uncertainties. A report on the data that were focused on this objective was previously published [5]. Other objectives included exploring a range of material types and exposure conditions, in which case the tests were not conducted with as much of a focus on replicates.

Table 1 shows some details of the samples tested. Flat rectangular samples were 23 × 11.5 cm at the solar furnace, and 90 × 120 cm at the solar tower. All flat samples were oriented vertically in a sample holder of the same size, with the focal point centered horizontally on the samples.

Solar tower samples were typically exposed at the center of the sample vertically, and solar furnace samples were typically exposed 5-6 cm below the top of the samples. Many other samples were more variable and applied forms of the materials suited to a similarly scaled exposure. The samples included variable thicknesses and other parameters, some of which are indicated in Table 1. Solar furnace tests were conducted in a partial enclosure with ambient openings at the top and at the front face that reduced the influence of wind on the samples. Samples were generally not backed by insulation, and in some cases back-side IR imagery was taken or thermocouples were attached giving a sense of the temperatures generated by the exposure. Solar tower tests were exposed to ambient winds. PMMA and HIPS samples were backed by insulation to minimize convection and radiation on the backside and simplify the thermal transport to enable modeling. Posterboard, canvas fabric, and aluminum samples were mounted with the back exposed. The tires, trees, trashcans, patio chairs, and upholstered chairs were mounted free-standing on custom support structures. Further details on the shape, size, characterization, and orientation of the samples are available in the test documentation and in other reports detailing results from this test series [5-9].

Table 1. Sample details regarding the reported Solar Tower (ST) and Solar Furnace (SF) experiments

Category	Sub-category	Details	Absorptivity
Cellulosic	Biomass	Green pine needles (bundle or mat, collected from a ponderosa pine less than a day before exposure, approximately 95% moisture content);	0.46
		Dry pine needles (bundle or mat; collected from the ground under a ponderosa pine, approximately 6% moisture content)	0.34
		Wheat (approximately 6% moisture content)	0.35
		Dry tumbleweed (approximately 12% moisture content)	0.64
		Soaked tumbleweed collected from a dead specimen (approximately 20% moisture content)	0.64
		Green tumbleweed (cut immediately before exposure, approximately 260% to 400% moisture content);	0.76
		Pinon pine tree (well-watered; cut within two hours of exposure)	0.6
	Paper	Posterboard	0.55 to 0.65
		Bundled paper	0.13
		Cellulose*	0.16
	Fabric	Olive canvas fabric, flame retardant and rain retardant	0.92
	Wood	Walnut veneer	0.5

Synthetic polymer	PMMA	Poly-methyl methacrylate (Plexiglas), black*	0.96
	HIPS	High impact polystyrene, black*	0.94
	Mixed Polymers	Vinyl siding, black	0.66
		Polypropylene chair	0.92
		Polyethylene trash can	0.95
		Synthetic rubber tires	0.9
		EPDM rubber swing seats	0.94

*Naturally white cellulose was blackened with a light coating of carbon consistent with Martin's methods; the polymer materials selected were made with black pigments mixed into the plastic

The solar and IR reflectivity of the samples were measured using a Surface Optics Corporation 410-Solar Visible/NIR Portable Reflectometer and a Surface Optics Corporation ET-100 Thermal Handheld Emissometer, respectively. The solar reflectometer measures the 20° incident total reflectance at seven sub-bands of 335–380, 400–540, 480–600, 590–720, 700–1100, 1000–1700, and 1700-2500 nanometers of a sample. Similarly, the thermal emissometer measures directional reflectance at two incidence angles, 20° and 60°, in six thermal sub-bands of 1.5–2.0, 2.0–3.5, 3.0–4.0, 4.0–5.0, 5.0–10.5, and 10.5–21.0 micrometers.

Some materials, including PMMA and some of the biomass samples, were observed to transmit some of the incident radiation through the samples. These materials absorb radiation in-depth within the material. Our absorptivity measurements cannot distinguish between surface and in-depth absorption.

2.1 Instrumentation

A variety of instrumentation was deployed for the tests. For this paper, highlights of the instrumentation are outlined only. Details on the instrumentation are available in the corresponding test phase documentation [6-9]. Each test included the following:

1. Pre- and post-test flux measurements to confirm the imposed thermal environment, and characterization of the day, time, and configuration of the flux source
2. Multiple angle fiducially accurate video imagery from standard, high-speed, and filtered optical cameras
3. Atmospheric data from weather stations to confirm the ambient conditions
4. Pre- and post-test photography
5. A temporal fiducial to allow post-test synchronization of instrumentation results from various sources
6. Controls output containing data on the temporal sequence for each test
7. Pre- and post-test weight of samples

Additional measurements/sensors were included in some tests to provide test information that can be utilized for determination of ignition and test characterization. These include:

1. Strategically mounted thermocouples for temperature measurements
2. IR camera imagery for thermal response
3. Witness strings as local air flow indicators

4. Post-test 3D scanning for digital re-construction of the thermal crater

Ignition and burn times are key to the analysis presented in this paper. These were deduced through post-test analysis of the video imagery. Ignition was often discernable through the observed flames in the video output. In some tests, the pyrolysis emissions obscured direct views of the ignition. The ignition event usually included a rapid increase in the motion of the pyrolysis gases/emissions, in which case the flames were not directly observed but inferred based on the motion of the opaque gases/emissions and the presence of flaming later in the video. Pyrolysis initiation was potentially confounded by a water vapor cloud created by evaporation from water content in some source materials. Mindful of this potential, analysts used judgement to interpret the pyrolysis initiation time by examining the coloration, chronology, and form of the cloud and the surface using video frame images such as those later shown in Figure 7.

2.2 Characterization of the Environment

Tests were conducted within a few hours of solar noon on clear (nearly cloudless) days with constant direct normal irradiation with variation of less than 3% as measured by a normal incident pyrheliometer. The environment was characterized using pre- and post-test analysis of heat flux instrumentation to verify the test conditions. Because of the response time of the test facility hardware, the imposed flux was a ramp to a constant hold, and a ramp back down to ambient.

Fluence magnitude was a target condition, which explains the regularity of intervals in some of the fluence conditions imposed on the samples. Fluence targets were usually round numbers, however post-analysis sometimes adjusted these away from the target values. For this paper, exposures are simplified to a fluence condition. Solar Furnace fluence was applied over a roughly 4-6 cm diameter spot [8], Solar Tower exposures varied spatially, but spanned the samples. Peak flux and fluence were centered on each sample. Efforts were made to account for spatial and temporal variations in the transient flux environment.

Tests were conducted at different times of the year in an outdoor environment. Ambient temperatures for two Solar Furnace test series conducted in July/August were 20-35ºC. The second Solar Furnace phase was conducted in February/March, and mid-day ambient temperatures were between 5-25ºC. The Solar Tower tests were conducted from August-November, and ambient temperatures varied between 10-30ºC. Post-processing of the data has not suggested a significant effect of the initial ambient temperature on any resultant parameters over the range of variation.

Repeatability of the tests was characterized for many of the detailed outputs from the tests. As a rule of thumb, we generalize about a 10% accuracy on flux, fluence, and thermal property data relating to these tests. A more detailed assessment of uncertainties can be found in other documentation sources relating to these datasets [5-9].

2.3 Video Analysis

Digital imagery were taken from both filtered and non-filtered cameras that were synchronized temporally with the exposures, which provides evidence of the material response beyond just ignition, which was point of focus in historical work. Two additional features or events were common to most materials and were extracted from the data. These features include the initiation of pyrolysis, which was evidenced by visible ejecta from the surface, and initiation of charring, evidenced by a change in coloration of the exposed samples. Fig. 7 shows examples of each of these observations. Cameras were positioned normal to the sample exposure, as well as perpendicular. The normal cameras were in an opening at the center of the parabolic mirror field. The perpendicular cameras were at the height of the exposure about 4 m away from the exposure. The video results were synchronized and were examined together to aid in the deduction of the timing of pyrolysis related events that are key to this analysis.

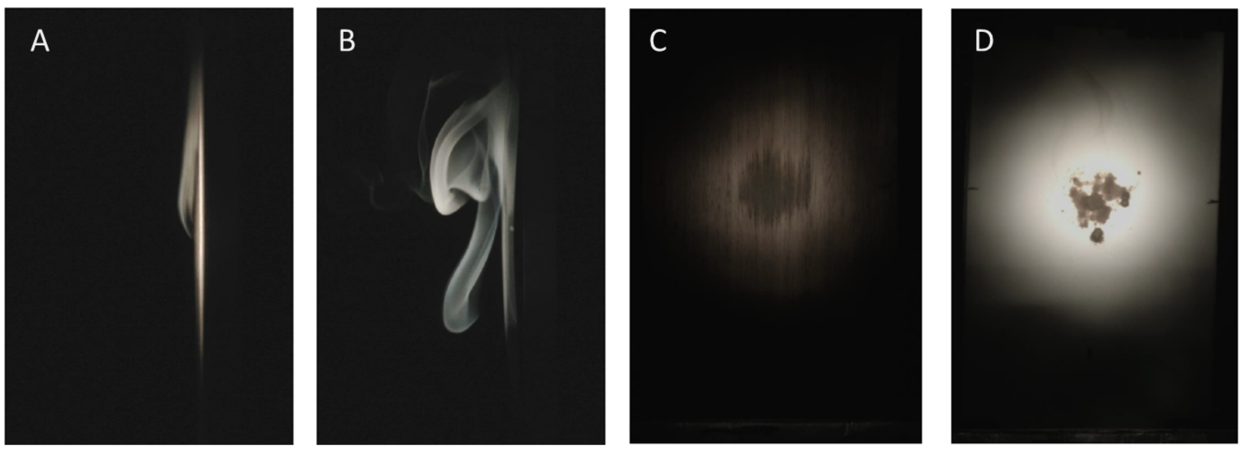

Fig. 7. Pyrolysis of walnut veneer (A) and high-impact polystyrene (B) as observed from the filtered side-view camera. Charring of walnut veneer (C) and cellulose pulp (D) samples as observed by the front-facing filtered camera. All images were captured after (≈ 100 ms) observed behavior began.

Key parameters were deduced from the time synchronized video and the characteristic exposures (as illustrated in Fig. 2) for parameter analysis. Fluence was the integrated flux for the full exposure from opening of the shutters to closing them. Flux was taken as the peak (maximum) flux. Time to pyrolysis and ignition were in most cases easily identified from review of the time coordinated images. Absorptivity was normally selected to be the un-charred value as deduced either from reference tables, or deduced from measurements taken with Surface Optics Corporation 410-Solar Visible/NIR portable Reflectometer and a ET-100 Emissometer. Heat flux and fluence were based on shutter calibrations, and the characterization flux measurements detailed in the prior section.

Onset of pyrolysis was captured by noting the time from test start at which the plume began to emerge from the high-speed imagery. This could be related to the exposure flux and fluence through the characterized exposures for each shot as illustrated for two shots in Fig. 2.

2.4 Ignition and Pyrolysis Thresholds

We have previously used a thermal surface temperature model for predicting the general ignition threshold shape of the Martin et al. work. The derivation is found in [9]. The derivation is based on a Green's function-based expression for the non-dimensional surface temperature of an inert solid heated by a constant load (q''_o) [11]:

$$\frac{k[T(x=0,F_O)-T_i]}{\alpha_o q_o'' L} = Fo_{th} + \frac{2}{\pi^2}\sum_{m=1}^{\infty}\frac{1}{m^2}\left(1-e^{-m^2\pi^2 Fo_{th}}\right) \quad (3)$$

The threshold normalized fluence (Q^*_{th}) is a function of the threshold temperature rise (ΔT_{th}) and a function uniquely dependent on the threshold Fourier number (Fo_{th}), which can be expressed as:

$$Q^*_{th} = q^*_{th} Fo_{th} = \Delta T_{th} f(Fo_{th}) \quad (4)$$

where the function is derived from Green's function as:

$$f(Fo_{th}) = \frac{Fo_{th}}{Fo_{th} + \frac{2}{\pi^2}\sum_{m=1}^{\infty}\frac{1}{m^2}\left(1-e^{-m^2\pi^2 Fo_{th}}\right)} \quad (5)$$

Here q^*_{th} is the normalized flux, and m is the index of summation. This theory represents a possible form for a predictive semi-empirical model for both ignition and for pyrolysis initiation. It has been shown to reasonably reproduce ignition thresholds originally determined by Martin et al. and could also represent the initiation of pyrolysis threshold at lower temperature rise conditions.

Some samples were observed to transmit some of the incident flux through the back of the samples. This was the case for some not fully opaque polymers, and some of the paper and biomass samples. Thinner samples also were more prone to exhibit this behavior. The analysis is done here assuming full absorption of the incident flux, which in some isolated cases may be a source of error. Occurrences of this were generally avoided by selecting samples not prone to these issues.

3. Results

Fig. 8 shows cellulosic material ignition events (red) and initiation of pyrolysis events (black). There is not always a corresponding ignition marker (red symbol) for every pyrolysis initiation marker (black symbol). There were tests that did not achieve ignition. They contribute pyrolysis initiation data, but do not contribute to the ignition data. Solid markers indicate tests that were performed at larger scale at the Solar Tower. The green dashed trend line is a rough approximation of the cellulose ignition threshold deduced by Martin's historical work, above which ignition is anticipated (as shown in Fig. 1). Keep in mind that the Martin data plotted in Fig. 1 are for thresholds and that each of their data points represents a compendium of many shots. The ignition markers in this work in Fig. 8 generally follow this same trend, although there are a fair number of cases where the ignition measurements deviate from the expected trend by as much as a factor of 3-4. The variability in the samples (color, size, moisture) is believed to be the most significant contributor to the spread. For example, the paper that ignited at the highest scaled fluence was white and bundled, whereas other darker paper-like materials ignited more readily. Since replicate tests were run, there is indication of the test variability inherent in the plots. Shot-to-shot variability is generally lower than observed in the spread due to materials. The fabric, one of the other most significant outliers from the trend lines, was treated with a fire retardant which is also expected to delay ignition.

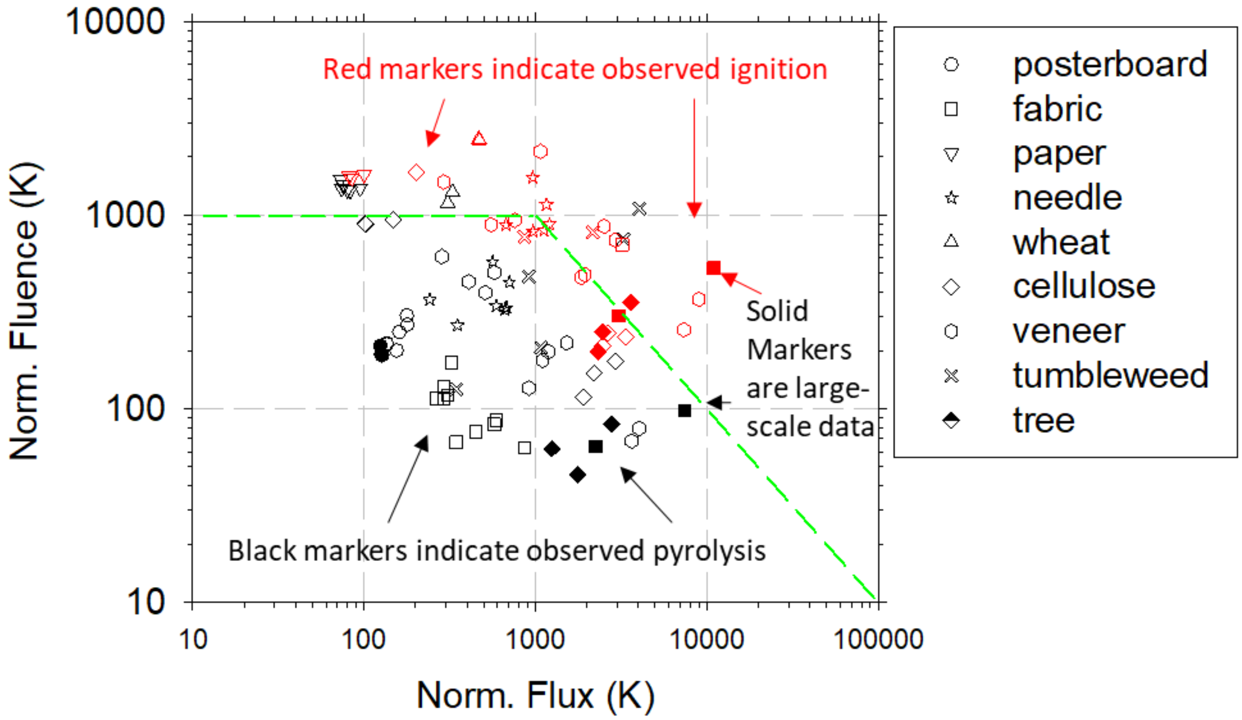

Fig. 8. Cellulosic material test results mapped to scaled flux/fluence.

The initiation of pyrolysis is shown with black markers. These generally fall below the green cellulose-based ignition trend lines with a few exceptions. The bundled paper did not start to pyrolyze until after the ignition threshold had been passed for blackened cellulose paper. Ignition often followed very shortly thereafter. Two of the tumbleweed samples also did not start to pyrolyze until well above the Martin threshold, and these were green, moist samples. The dry and moistened tumbleweed samples behaved more consistently with the expected trends including the trends of Martin et al. and of the rest of the dry cellulosic materials.

Note the general trend of pyrolysis initiation to ignition is mostly upward and slightly to the right in these plots, much like illustrated in the bottom plot of Fig. 2. This can be seen more easily in the more sparse dataset data such as trees, needles, and paper. Another noteworthy observation is that the initiation of pyrolysis is not generally a uniform distance separated from the ignition threshold in the plots. The general spread of these data is best illustrated in the variety of walnut wood veneer tests performed. Thickness and exposure were varied to achieve significant spreading of the data across the mapped regions of this plot. The ignition points generally follow the cellulose trends with some of the ignitions occurring a little above the ignition threshold lines. The initiation of pyrolysis is similarly grouped, and trend with a similar slope as the Martin et al. transient ignition branch. These are examined in more detail a little later in this paper.

Fig. 9 shows a similar plot of synthetic polymeric ignition events (red) and initiation of pyrolysis events (black). Solid markers (filled) indicate tests that were performed at larger scale at the Solar Tower. These tests were almost all performed with ignitions in a regime to the right of the inflection point for the ignition trend suggested by the dashed green line. Even though Martin's construct for the ignition threshold was derived uniquely for cellulose, the general trending appears to hold for many of the synthetic polymers as well. Ignitions for vinyl and tires are slightly inside the cellulose trends, while the remainder of the synthetic polymers were more resistant to ignition compared with cellulose, igniting beyond the general cellulose trend. The general downward diagonal trend found for cellulosic materials is also evident in the synthetic polymer results. There are insufficient data here to deduce trends for specific materials, but the general diagonal trending above 1000 K Normalized Flux for some of the polymers is apparent.

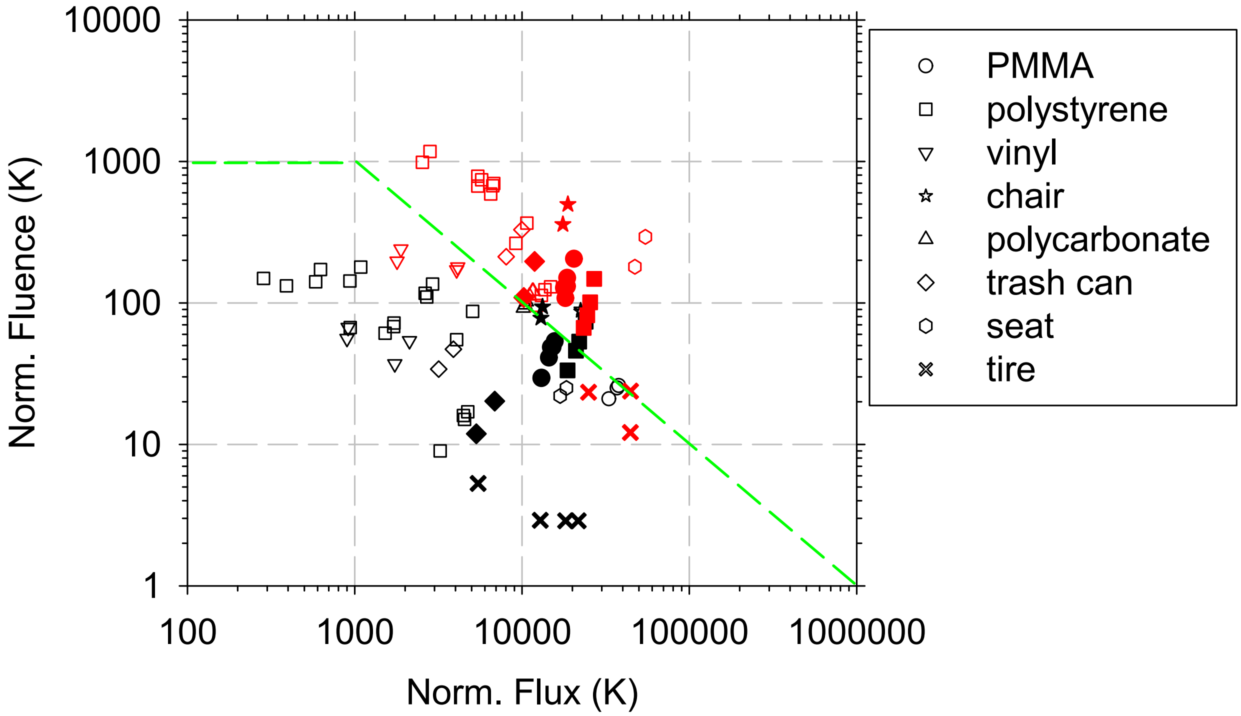

Fig. 9. Synthetic polymer material test results mapped to scaled flux/fluence.

Polystyrene for the synthetic polymers was treated like the veneer for the cellulosic materials, in that it was varied across the range of the map to a greater degree for a larger number of samples. The Solar Furnace ignitions are 10-20% above the cellulose ignition threshold. The Solar Tower ignitions fall in line similar to the smaller-scale solar furnace tests relatively well. The initiation of pyrolysis data follow a similar diagonal trend, with the Solar Tower data outside the main trend of the rest of the Solar furnace data. A prior analysis [5] has noted a propensity for scale effect for ignition of some materials, a feature not identified in the historical datasets. This is not particularly apparent in this figure, as the large-scale solar tower tests tend to align relatively well with the general trends of the solar furnace data from smaller-scale tests. Note that the PMMA tests exhibited pyrolysis initiation at small-scale, but never ignition. At the large-scale at similar exposure conditions, ignitions were observed.

At a minimum, the test matrix generally involved duplicate testing of each sample at each condition (this or a ramp in flux conditions with one test at each increment to establish a trend). Certain tests involved more than two repeats. While test data here contribute to the identification of ignition and pyrolysis initiation thresholds, more extensive testing is needed to form a comparable map to that found in Fig. 1 from Martin et al.'s work.

Isotherms for temperature rise plotted onto the normalized construct suggest possible model thresholds that follow the critical temperature rise model (Equations 1-2) that appears to successfully reproduce ignition thresholds for cellulose. A few material types with a large number of tests are specifically examined. Figure 10 shows the veneer ignition and pyrolysis initiation data isolated and plotted with candidate threshold temperatures ranging from 350-500ºC in increments of 50ºC. Ignoring one outlier, the 500ºC threshold curve appears to capture what may be a good pyrolysis initiation threshold for the existing data. The ignition data appear to trend similar to the cellulose data of Martin et al., with an inflection at both 1000K normalized fluence and flux. One might deduce from this trend that the threshold for initiation of pyrolysis is in the 350-400ºC range taking the most extreme datum, or about 500ºC if that point is deemed an outlier. This threshold could then be used with Equations 4 and 5 to deduce a threshold normalized flux for pyrolysis initiation via the relation relating normalized flux, normalized fluence, and the Fourier number shown in the first relation from the left in Equation 1.

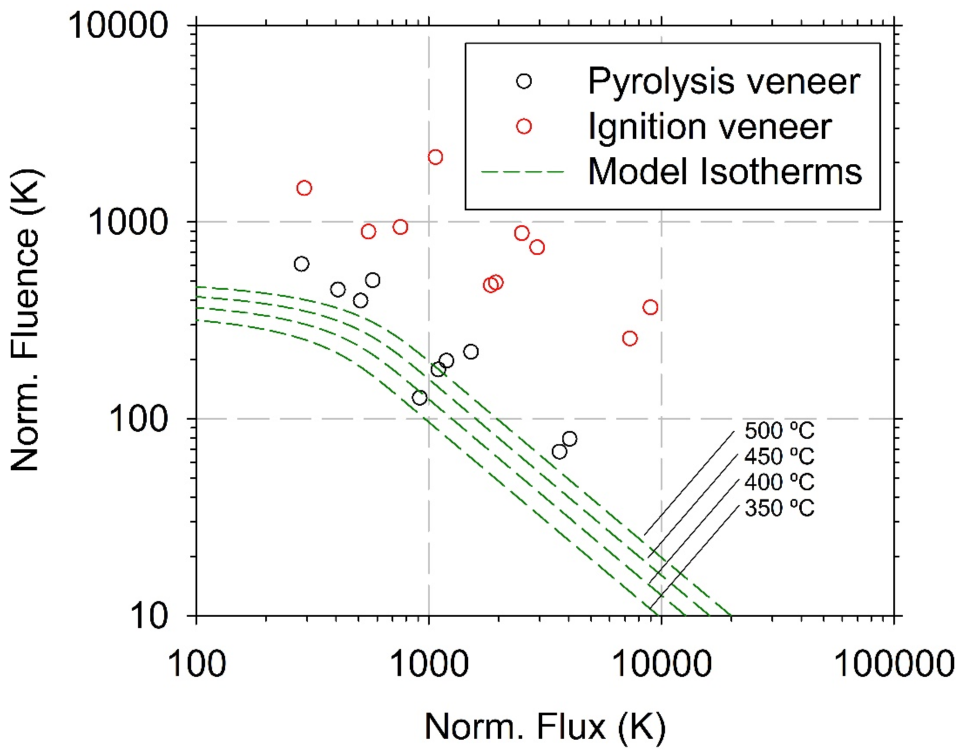

Fig. 10. Wood veneer data compared to model isotherms from 350-500ºC

Similarly, the HIPS polystyrene data can be evaluated for pyrolysis initiation thresholds as shown in Fig. 11. Here the range of candidate curves vary from 250-400ºC. The smaller-scale SF data suggest a threshold of ≈250ºC depending on whether the lowest datum is an outlier, but the larger-scale data appears to fall close to the limits of the spread of the smaller-scale data, with a bias towards the upper-right in Fig. 11. The ignition threshold appears to be shifted outward from what was found for cellulose via the Martin data, and trends more consistently with scale than did the pyrolysis initiation data. The outward trend is not unexpected given that the polymer materials are different than the cellulose. One would expect the possible need to adapt the ignition thresholds to the specific materials being exposed via the temperature rise parameter. We refrain from attempting a more formal fit to the data given the general sparsity of our current dataset compared to the historical ignition data for cellulose. The data are sufficient, however, to note that the general trend of the data is largely consistent with the model trend, and that with additional targeted data, one might recommend temperature thresholds that match ignitions for various material types to enable a specific ignition threshold curve for any number of candidate materials for ignition modeling. This might involve an increasing number of realizations with more sample thicknesses and exposure environments.

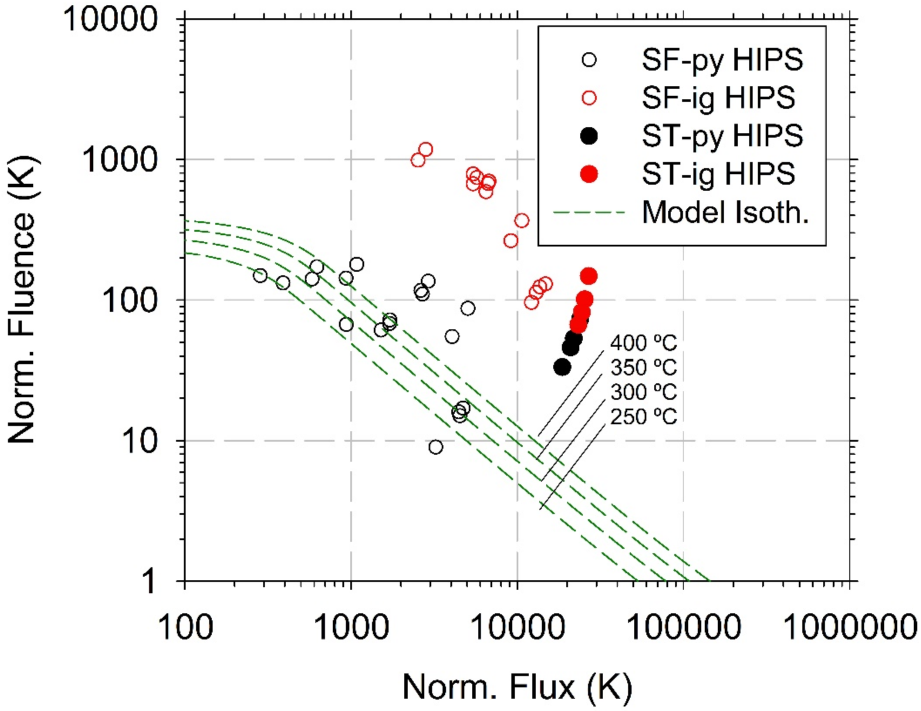

Fig. 11. Polystyrene data compared to model isotherms from 250-400ºC.

4. Discussion

The recent ignition data from the concentrating solar facilities at Sandia provide updated perspective on the response of materials subjected to high flux exposures. Figs. 8-9 show individual test results grouped as cellulosic and engineered polymers. These figures illustrate the general variety of response of materials to the high-flux environment. While the normalization of flux and fluence and the general construct found from the historical cellulose tests appears to collapse data from a single material, the variety of real materials potentially involved in an ignition event are expected to exhibit a more widely ranging response. Cellulosic materials tended to generally follow the ignition trends of the historical data with variations depending on moisture, shape, and treatments. The polymers were generally more uniform materials from sample to sample, but still exhibit a significant spread. Engineered polymers exhibit a range of ignition thresholds depending presumably on constituency of the polymer.

The initiation of pyrolysis was extracted from the same tests and falls inside (lower and to the left) of the ignition data on the normalized flux/fluence plots. An effort was made to produce a range of data spanning the plot across the two linear regimes by varying the exposure magnitudes and material thicknesses. Our data predominantly fell to the right of the inflection point on the diagonal near 1000 K normalized flux, and largely follows the same diagonal slope as does the historical cellulose ignition data. A similar diagonal trend is discernable in the pyrolysis initiation data results from both our tests and from Martin's work, which suggests pyrolysis initiation thresholds trend similarly to the ignition thresholds for high-flux exposures. This feature is better illustrated in the isolated veneer and HIPS data in Figs 10-11, where the Green's function-based model shows promise for producing a generalized trend for a pyrolysis initiation threshold in the high flux regime. The scatter in these data is relatively high. For threshold determination, one would focus on the inner-most datapoints among replicates to define an inner-threshold. This approach is presumably what was done by Martin et al., as their data points that are shown in Fig. 1 are threshold values determined from replicate tests, and not individual test results as are the subsequent data in similar plots. The Martin data presumably exhibited scatter much like the present results, although the contributing data to the thresholds were not as extensively reported.

Predictivity of material response to a high flux environment for a variety of materials is challenging. Ignition thresholds are well characterized for blackened cellulose, but few other materials have similar depth of information. Figs. 8-9 suggest a range over which ignitions and pyrolysis initiations occur for a more general suite of materials. Assuming the physical mechanistic drivers remain similar, this construct may be applicable for a range of materials. Thus, model determination may be accelerated by reliance on a verified model form and fewer tests to characterize the relative scaling of the threshold curve. This general theoretical construct may work for many more materials than cellulose and enhance the ability to formulate a comprehensive ignition model. There are some exceptions, as we have observed our PMMA samples would not ignite at the solar furnace regardless of the flux/fluence. When we scaled up to the solar tower, PMMA ignited readily [6]. PMMA appears to rely on a gas-phase ignition that is enhanced in thicker pyrolysis plumes.

Ignitions in more common fire conditions (low-flux by the convention of this paper) will not be widely expected to trend according to the model form of Equation 5, as the historical data suggest that ignitions further to the left in the normalized flux/fluence plots reach a regime where convection and conductivity become an increasingly important factor to ignition. This transition could be linked to a Fourier number, with the data and models suggesting at present that the regime of validity will be for all scenarios with $Fo<1.0$ and possibly for scenarios with $Fo<10$-100. A greater variety of data are required for more precise recommendations, as the Martin et al. datasets focused to a much greater extent on ignitions in the higher Fourier number regimes.

While the utility of the current model is limited to the high-flux regime, it represents an improvement on the prior state of the theory. Ignitions in Figure 1 were largely determined from the same scale, and we have since shown that there are clear scale effects for some materials that manifest as different flux ignition thresholds [6]. These effects likely relate to the plume dynamics of the pyrolysis gases being different for the different scales, and the thickness of the pyrolysis gas layer relating to ignition through attenuation of the incident flux.

At larger scales, the pyrolysis plumes can be larger and thicker, absorbing more incident radiation, and providing a larger area and volume over which ignitions can start. Indeed, videos suggest varying opacities for the pyrolysis plumes emitted from exposed samples depending on material type, and this variability most likely has some relation to the thresholds and if not then certainly the mechanisms whereby ignitions occur. Videos also suggest at large-scale that the ignition phenomena might be more than just a result of surface temperatures reaching ignition thresholds, with some indications of gas-phase ignitions in a few of the test videos. These dynamics that relate to additional test factors cannot be represented in the ignition thresholds using the normalized flux and fluence constructs alone, but the pyrolysis and char initiation thresholds will be less affected by scale and possibly environmental issues. Consequently, the pyrolysis initiation represents an improved indicator of the state of the exposed material trending towards ignition and could be a feature of lower uncertainty to evaluate when trying to characterize the response of materials to high flux scenarios. The pyrolysis initiation threshold also represents an indication of the start of thermal damage of the materials due to an exposure. It may additionally be relevant to forensic analysis when trying to determine the magnitude of an exposure based on material response, or fire propagation modeling. Propagation modeling will depend on the absorptivity of the local materials to accurately predict flaming spread through non-ignited but previously exposed materials.

5. Conclusions

Recent high heat flux datasets from concentrated solar exposures on a variety of materials provide new data for the response of materials to very high (>200 kW/m^2) radiant exposures. Using the historically suggested construct of normalized flux and fluence, the data from the current tests are shown to be mostly consistent with the historical work in regard to cellulose ignition. Like ignition, the initiation of pyrolysis (a feature not measured in historical datasets) appears to follow a trend of lower energy required at high flux conditions. Temperature rise isotherms from a Green's function-based model for surface response to an exposure seems to fit the general trend of both the ignition and pyrolysis initiation thresholds, providing a promising theoretical construct for capturing material variations and grounds for future modeling. More data are needed for complete and accurate fits that include increased variations in exposures and material types.

Acknowledgements

This article has been authored by an employee of National Technology & Engineering Solutions of Sandia, LLC under Contract No. DE-NA0003525 with the U.S. Department of Energy (DOE). The employee owns all right, title and interest in and to the article and is solely responsible for its contents. The United States Government retains and the publisher, by accepting the article for publication, acknowledges that the United States Government retains a non-exclusive, paid-up,

References

[1] Martin, S., 1965, January. Diffusion-controlled ignition of cellulosic materials by intense radiant energy. In Symposium (International) on Combustion (Vol. 10, No. 1, pp. 877-896). http://dx.doi.org/10.1016/S0082-0784(65)80232-6

[2] Martin S. B. “Fire setting by nuclear explosion: A revisit and use in nonnuclear applications,” Journal of Fire Protection Engineering Vol. 14 No. 4, 2004, pp. 283-97. http://dx.doi.org/10.1177/1042391504044541

[3] Glasstone, S. and Dolan, P.J., 1977. *The effects of nuclear weapons*. DEPARTMENT OF DEFENSE WASHINGTON DC.

[4] Butler, C.P., Martin, S.B. and Lai, W., 1956. *Thermal Radiation Damage to Cellulosic Materials. Part II. Ignition of Alpha Cellulose by Square-wave Exposure* (No. USNRDL-TR-135; AFSWP-906; Project NS 081-001). Naval Radiological Defense Lab., San Francisco.

[5] Brown, A.L., Engerer, J.D., Ricks, A.J., Christian, J., Yellowhair, J., "Datasets for Material Ignition from High Radiant Flux," Vol 120, Fire Safety Journal 2021, p. 103031. https://doi.org/10.1016/j.firesaf.2020.103131

[6] Brown, A.L., Engerer, J.D., Ricks, A.J., and Christian, J.M., “Scale Dependence of Material Response at Extreme Incident Radiative Heat Flux,” The 2018 ASME/AIAA Joint Thermophysics and Heat Transfer Conference, Atlanta, Georgia, June 25-29, 2018.

[7] Brown, A.L., Engerer, J.D., Ricks, A.J., and Christian, J.M., (2019) “Ignition from High Heat Flux for Flat Versus Complex Geometry”, 9th Symposium on Fire and Explosions Hazards, April 21-26, St. Petersburg, Russia, pp. 970-979.

[8] Ricks, A.J., Brown, A.L., and Christian, J.M. “Flash Ignition Tests at the National Solar Thermal Test Facility,” The 2018 ASME/AIAA Joint Thermophysics and Heat Transfer Conference, Atlanta, Georgia, June 25-29, 2018.

[9] Engerer, J.D., Brown, A.L., and Christian, J.M. “Ignition and Damage Thresholds of Materials at Extreme Incident Radiative Heat Flux,” The 2018 ASME/AIAA Joint Thermophysics and Heat Transfer Conference, Atlanta, Georgia, June 25-29, 2018.

[10] Zepper, E.T., Brown, A.L., Scott, S.N., “Model Validation Exploration for Reacting Solids Exposed to High Heat Flux Environments,” 2019 WSSCI Fall Technical Meeting Organized by the Western States Section of the Combustion Institute October 14–15, 2019 Albuquerque, New Mexico.

[11] Cole, K., Beck, J. V., Haji-Sheikh, A., and Bahman, L., Heat Conduction Using Green’s Functions, Taylor & Francis, 2011.